ATAD5 regulates the lifespan of DNA replication factories by modulating PCNA level on the chromatin

Kyoo-young Lee,[1] Haiqing Fu,[2] Mirit I. Aladjem,[2] and Kyungjae Myung[1]

[1]Genome Instability Section, Genetics and Molecular Biology Branch, National Human Genome Research Institute, National Institutes of Health, Bethesda, MD 20892
[2]DNA replication group, Laboratory of Molecular Pharmacology, Center for Cancer Research, National Cancer Institute, National Institutes of Health, Bethesda, MD 20892

Temporal and spatial regulation of the replication factory is important for efficient DNA replication. However, the underlying molecular mechanisms are not well understood. Here, we report that ATAD5 regulates the lifespan of replication factories. Reduced expression of ATAD5 extended the lifespan of replication factories by retaining proliferating cell nuclear antigen (PCNA) and other replisome proteins on the chromatin during and even after DNA synthesis. This led to an increase of inactive replication factories with an accumulation of replisome proteins. Consequently, the overall replication rate was decreased, which resulted in the delay of S-phase progression. Prevalent detection of PCNA foci in G2 phase cells after ATAD5 depletion suggests that defects in the disassembly of replication factories persist after S phase is complete. ATAD5-mediated regulation of the replication factory and PCNA required an intact ATAD5 ATPase domain. Taken together, our data imply that ATAD5 regulates the cycle of DNA replication factories, probably through its PCNA-unloading activity.

Introduction

The eukaryotic sliding clamp, proliferating cell nuclear antigen (PCNA), performs critical functions during DNA replication as a processivity factor for DNA polymerases as well as a docking site for many post-DNA synthesis proteins (Moldovan et al., 2007). During DNA replication, two PCNA clamps are loaded at the origin and slide on the leading strand in both directions until replicon synthesis is completed. Simultaneously, PCNA begins to be loaded on the lagging strand for bi-directional DNA synthesis and is repeatedly loaded for synthesis of each Okazaki fragment. Considering the limited amount of PCNA compared with the number of Okazaki fragments to be synthesized, PCNA needs to be unloaded for recycling. It is not clear when PCNA unloading occurs because PCNA needs to remain on the chromatin to mark replicated DNA for proper chromatin assembly (Shibahara and Stillman, 1999).

During S phase of eukaryotic cells, several neighboring replication origins are simultaneously fired and replicated at a specific location in the nucleus called the replication factory (Berezney et al., 2000). Many replication proteins accumulate at the replication factory and can be visualized as foci by immunostaining PCNA (Bravo and Macdonald-Bravo, 1987). The lifespan of replication factories from gradual buildup to disassembly, as determined by PCNA foci, ranges from minutes to hours (Leonhardt et al., 2000). Due to its intrinsic property as a scaffold, PCNA is believed to play a major role in the replication factory. PCNA left behind after Okazaki fragment synthesis has been proposed as a binding platform for other replication proteins (Sporbert et al., 2005). Thus, the balance and the timing between PCNA loading and unloading might determine the cycle of a given replication factory.

PCNA is loaded onto DNA by the replication factor C (RFC) complex, composed of five subunits, RFC1–5 (Majka and Burgers, 2004). PCNA unloading activity of RFC was also reported in vitro (Cai et al., 1996; Yao et al., 1996; Shibahara and Stillman, 1999). Eukaryotic cells have three RFC-like complexes (RLCs) composed of RFC2–5 and one alternative subunit that replaces the canonical RFC1: RAD17, CTF18, or ELG1 (ATAD5 in human). RAD17–RLC loads the RAD9–RAD1–HUS1 (9–1–1) complex at damaged DNA for checkpoint activation (Green et al., 2000; Lindsey-Boltz et al., 2001; Majka and Burgers, 2003; Navadgi-Patil and Burgers, 2009).

Correspondence to Kyungjae Myung: kmyung@mail.nih.gov

Abbreviations used in this paper: EdU, ethynyl deoxyuridine; PCNA, proliferating cell nuclear antigen; RFC, replication factor C; RLC, RFC-like complex; RPA, replication protein A; UAF1, USP1-associated factor; USP1, ubiquitin-specific protease 1.

The Rockefeller University Press $30.00
J. Cell Biol. Vol. 200 No. 1 31–44
www.jcb.org/cgi/doi/10.1083/jcb.201206084

CTF18–RLC is important for sister chromatid cohesion (Mayer et al., 2001; Merkle et al., 2003). CTF18–RLC was reported to have PCNA loading/unloading activity in vitro (Majka and Burgers, 2004).

Elg1p was first identified as a suppressor of genomic instability in budding yeast (Bellaoui et al., 2003; Ben-Aroya et al., 2003; Huang et al., 2003; Kanellis et al., 2003; Smith et al., 2004). Elg1p is involved in DNA replication, DNA recombination, and telomere length regulation (Banerjee and Myung, 2004; Smolikov et al., 2004). The human homologue of yeast Elg1 is encoded by the *ATAD5* gene. ATAD5 regulates PCNA deubiquitylation by recruiting the ubiquitin-specific protease 1 (USP1)–USP1-associated factor (UAF1) complex to ubiquitylated PCNA (Lee et al., 2010). Recently, we reported that ATAD5 is important for genomic stability and suppress tumorigenesis both in mice and humans (Sikdar et al., 2009; Bell et al., 2011). In these studies, we found that unlike the *Usp1*-null mice (Kim et al., 2009), the *Atad5*-null mice die early in embryogenesis, which suggests that ATAD5 has another function important for embryonic survival. Unlike other clamp loaders, PCNA loading/unloading activity by ATAD5–RLC has not been investigated. However, several indirect evidences from yeast studies suggest a possible role of Elg1p–RLC in PCNA regulation during DNA replication (Kanellis et al., 2003; Kim et al., 2005; Parnas et al., 2010; Kubota et al., 2011). Therefore, we investigated the role of ATAD5 in PCNA regulation in more detail. Here, we report that ATAD5 knockdown leads to an increase of DNA synthesis–defective replication factories where replication proteins accumulate in a PCNA-dependent manner. ATAD5 actively regulates the dynamics of replication factories. Consistently, defects in ATAD5, especially in its ATPase function, result in a delay in the replication rate and cell cycle progression. We propose a connection between PCNA unloading and dismantlement of replication factories, both of which appear to be regulated by ATAD5–RLC.

Results

ATAD5 knockdown produces abnormally large PCNA foci

Based on the fact that physical interaction exists between ATAD5 and PCNA and that ATAD5 regulates PCNA ubiquitylation (Lee et al., 2010), we hypothesized that ATAD5 would affect the dynamics of PCNA during DNA replication. We investigated the staining pattern of PCNA in cells after depleting ATAD5 by siRNA. PCNA in the nucleus of replicating cells forms foci structures, termed replication foci, which represent replication factories where DNA is replicated (Celis and Celis, 1985). In both HeLa and RPE cells, even though similar PCNA foci patterns were observed in ATAD5 knockdown cells compared with control cells, the signal intensity was greater in the majority of ATAD5 knockdown cells (Fig. 1 A and Fig. S1 A). The quantified signal intensity of chromatin-bound PCNA foci was significantly higher in ATAD5 knockdown cells (Fig. 1 B and Fig. S1 B). Clear differences in the signal intensity of PCNA foci between ATAD5 knockdown cells bound to small beads and control cells bound to large beads prepared in a single slide chamber excluded the possibility of experimental variations (Fig. S1 C).

The distinctive spatio-temporal patterns of PCNA foci during S phase, including distribution, size, and shape can be used for classifying S-phase cells into subcategories (Nakayasu and Berezney, 1989; Hozák et al., 1994; Leonhardt et al., 2000). Using these criteria, we classified ATAD5 knockdown and control cells into early, mid, and late S phases (Fig. 1 A). The unusually brighter PCNA foci in ATAD5 knockdown cells were detected in all sub-S phases. Detail analysis of PCNA foci in early S phase, where PCNA foci can be easily measured, demonstrates significant increase in the signal intensity and the size of PCNA foci upon ATAD5 knockdown (Fig. 1, C and D; and Fig. S1 D). Taken together, PCNA accumulates on the chromatin and forms abnormally large foci structures when ATAD5 is depleted.

PCNA also forms foci when the replication machinery stalls at damaged DNA during S phase. DNA damage–induced PCNA foci can be distinguished from replication foci in early S phase by their colocalization with replication protein A (RPA), a single-strand DNA (ssDNA)–binding protein that accumulates at DNA damage–induced foci because the uncoupling of the helicase and replicative polymerases at stalled replication forks produces long ssDNA (Davies et al., 2008). In contrast to the colocalized PCNA and RPA foci in response to ultraviolet (UV) irradiation (Fig. 1 E), a portion of ATAD5 knockdown cells that had discrete PCNA foci did not contain RPA foci, indicating that the abnormally large PCNA foci observed after ATAD5 knockdown were not generated in response to DNA damage–induced ssDNA at stalled replication forks.

ATAD5 knockdown extends lifespan of replication foci

To examine the dynamics of PCNA in more detail, we monitored the GFP-fused PCNA (GFP-PCNA) stably expressed in a HeLa cell line (Leonhardt et al., 2000). Live-cell images obtained after ATAD5 knockdown were analyzed based on their GFP-PCNA foci patterns (Fig. 2 A). Similar to endogenous PCNA foci, the intensity of GFP-PCNA foci signal was increased in ATAD5 knockdown cells compared with control cells throughout the S phase (Fig. 2 A and Fig. S2). The duration of the GFP-PCNA–positive phase (from phase I to IV in Fig. 2 A) determined in each cell from the consecutive images showed that the mean duration of the GFP-PCNA–positive phase increased from 11.6 h in control cells to 16.3 h in ATAD5 knockdown cells (Fig. 2 B).

The consecutive images of the GFP-PCNA–positive phase for each cell were divided into four sequential phases (phase I to IV) according to the foci pattern (Fig. 2 A; Nakayasu and Berezney, 1989; Hozák et al., 1994). We divided the classical late S phase into two phases, phase III and phase IV, based on the observation that cells in phase IV did not have newly arising PCNA foci, but rather had diminished ones. This observation was more pronounced in ATAD5 knockdown cells. We also included phase V encompassing the span between phase IV and mitosis. In a normal cell cycle, phase V represents the G2 phase. We applied this classification to measure the duration time of each phase in detail (Fig. 2, C and D). However, due to the difficulty of classifying cells in transition from phase I to II

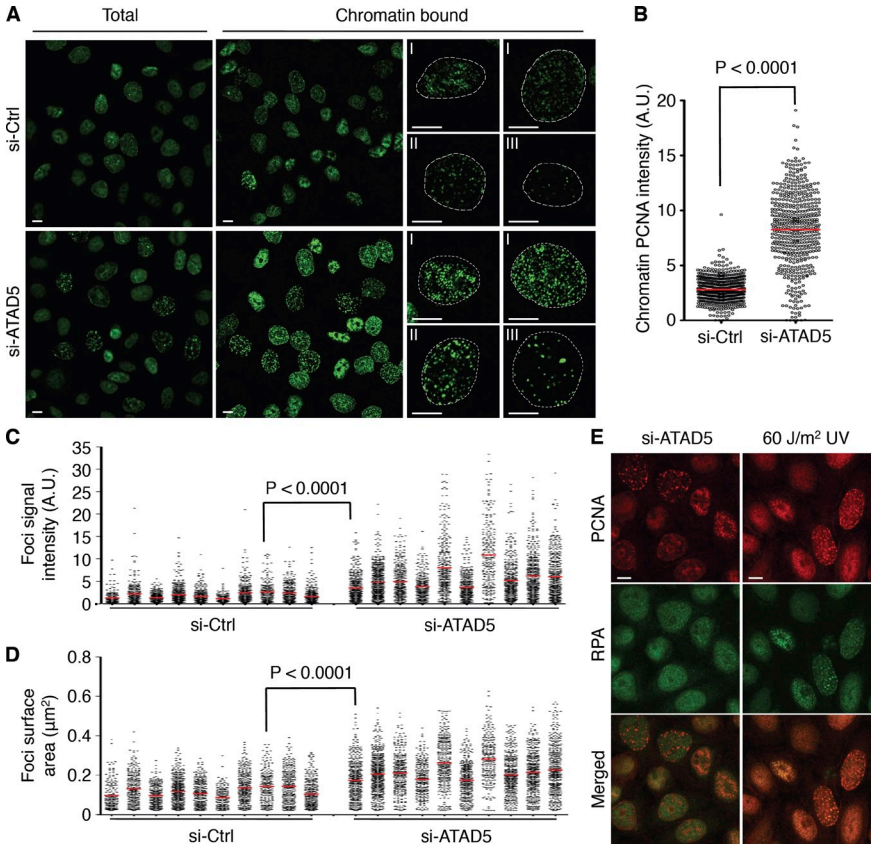

Figure 1. **ATAD5 knockdown generates abnormally large PCNA foci.** In all experiments, HeLa cells were transfected with *ATAD5* or control siRNA and analyzed after 72 h unless otherwise specified. (A) Cells were fixed with (chromatin bound) or without (total) a prior soluble protein extraction step, stained with anti-PCNA antibody, and analyzed by confocal microscopy. Dotted lines denote nuclear boundary determined by DAPI staining. I, II, and III denote early, mid, and late S phase, respectively. (B) Box blot showing the quantitation of chromatin-bound PCNA signal intensity. The data shown are from a single representative experiment out of three repeats. For the experiment shown, $n > 500$ in each condition. A.U., arbitrary unit; red bars in the graph, mean value; P, significance by *t* test. (C and D) PCNA foci in early S-phase nuclei ($n = 10$ in each condition) were quantitatively analyzed for foci signal intensity (C) and foci size (D). The data shown are from a single representative experiment out of three repeats. For the experiment shown, $n = 10$ for each condition. A *t* test was performed between the control knockdown cell with maximum mean signal intensity and size of PCNA foci and the ATAD5 knockdown cell with minimum. (E) Cells were fixed, stained with both anti-PCNA and anti-RPA antibodies, and analyzed by confocal microscopy. UV-irradiated cells were prepared in the same way as the positive control. Bars (all images): 5 μm.

as well as from phase II to III, we combined phase I through III for further analysis. The mean combined duration time of phase I through III was delayed by ATAD5 knockdown (12.7 h for si-ATAD5 vs. 11.1 h for si-Ctrl). However, the greatest difference was observed in phase IV, where ATAD5 knockdown increased the mean duration fourfold compared with control knockdown cells (3.2 h for si-ATAD5 vs. 0.8 h for si-Ctrl). We found that the duration time of phase V was shorter in ATAD5 knockdown cells compared with control (Fig. 2 D; 3.1 h for si-ATAD5 vs. 5.2 h for si-Ctrl), leading to a similar combined mean duration time of phase IV and V in both cell types (Fig. 2 E).

Replication foci appear and disappear at fixed positions with different cycling times (Leonhardt et al., 2000). We analyzed the lifespan and signal intensity of GFP-PCNA foci in the S phase of ATAD5 knockdown and control cells. GFP-PCNA foci in the ATAD5 knockdown cells with a long S-phase duration (over 16 h) displayed longer cycling times compared with control cells (Fig. 2 F). In contrast to GFP-PCNA foci with short lifespan in both ATAD5 knockdown and control cells, GFP-PCNA foci with a long lifespan (over 4 h) in ATAD5 knockdown cells began to appear in phase II (mid S phase), increased intensity to a plateau level, then maintained such level before disappearing in phase IV (Fig. 2, G and H). Taken together, these data indicate that ATAD5 knockdown extends the lifespan of PCNA foci.

Inactive replication factories remain in G2 phase by ATAD5 knockdown

Extended phase IV and shortened phase V after ATAD5 knockdown (Fig. 2 E) suggest that the entire or a latter portion of phase IV in ATAD5 knockdown cells might be in G2 phase. To test this possibility, we examined the staining pattern of cyclin B1 (Fig. 3 A), which accumulates in the cytoplasm throughout G2 phase (Pines and Hunter, 1989). We also labeled cells with BrdU, which is incorporated into replicating DNA. Cells in G2 phase are defined as positive in cyclin B1 and negative in BrdU signals. Under these criteria, there was no control cell at the G2 phase that had PCNA foci. In contrast, 28.9% of ATAD5 knockdown cells at the G2 phase had PCNA foci (Fig. 3, A and B; asterisk-marked cells). These data indicate that PCNA foci remain on the chromatin even after cells enter the G2 phase. We also concluded that the latter portion of phase IV in ATAD5 knockdown cells is in G2 phase.

A replication factory contains many proteins that are involved in DNA synthesis, repair, chromatin assembly, and sister chromatid cohesion (Berezney et al., 2000). PCNA functions as a platform for other proteins within the replication factory (Sporbert et al., 2005). We hypothesized that the PCNA foci found in the G2 phase after ATAD5 knockdown would represent inactive replication factories that contain other replication proteins. To test this possibility, we examined the staining pattern of replication proteins, which include DNA ligase 1, a chromatin-assembly protein CAF-1, and MRE11, another replisome-associated protein. In addition to the active replication factories with a BrdU signal, replication proteins also colocalized with PCNA foci having no BrdU signal in ATAD5 knockdown cells (Fig. 3 C). Taken together, these data show that ATAD5 knockdown causes inactive replication factories to remain on the chromatin even after cells enter the G2 phase, possibly in a PCNA-dependent manner.

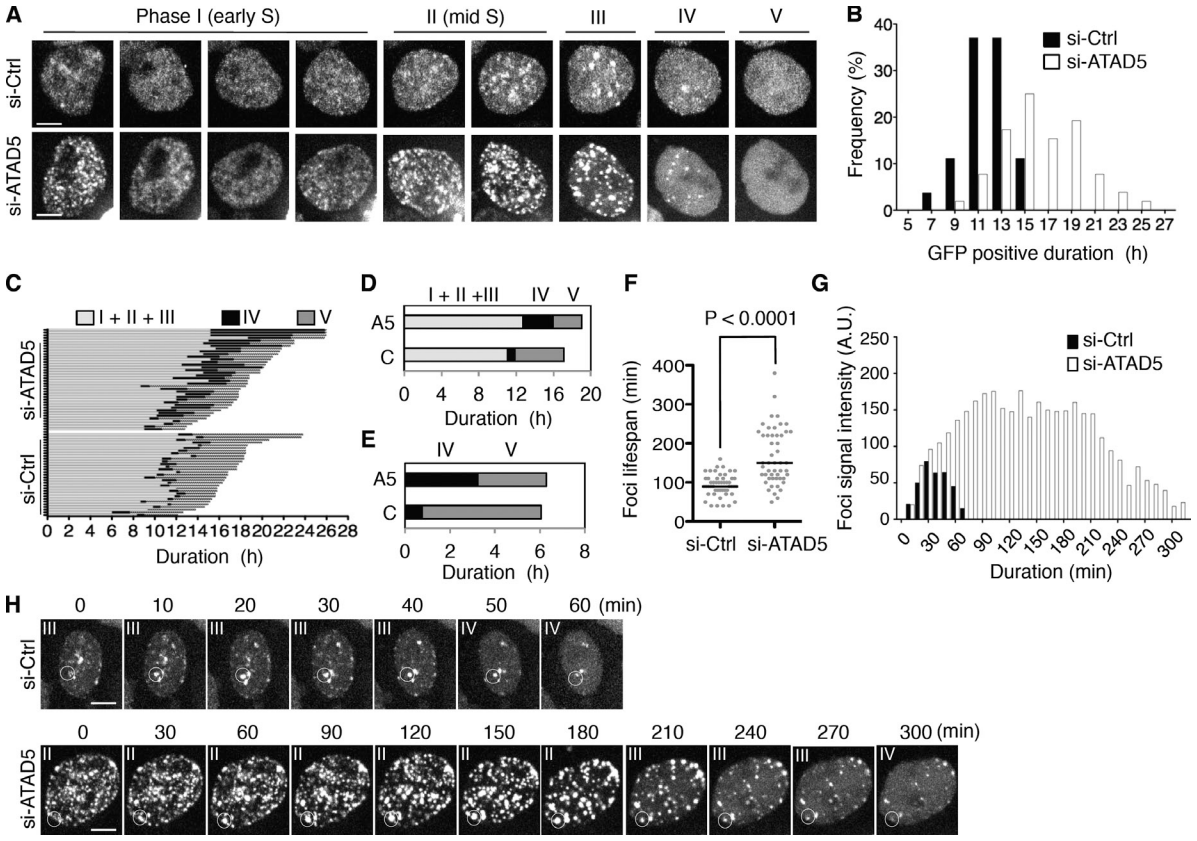

Figure 2. **ATAD5 knockdown extends lifespan of PCNA foci.** HeLa cells stably expressing GFP-PCNA were transfected with *ATAD5* or control siRNA. After 72 h, GFP images were taken using a spinning disc microscope. (A) The representative consecutive images of a GFP-positive cell with the classification used are displayed. Bars, 5 µm. (B–G) The data shown are from a single representative experiment out of two independent experiments. (B) The duration time of GFP-PCNA signal in each cell was measured (n = 51 for si-Ctrl cells; n = 50 for si-ATAD5 cells) and the frequency of distribution was displayed. (C) The duration time of each phase was measured (n = 31 for si-Ctrl cells; n = 37 for si-ATAD5 cells) based on the classification in A. (D and E) Mean duration time of each phase in C. A5, si-ATAD5; C, si-Ctrl; I–V, phase I–V. (F) The lifespan of PCNA foci was measured (n = 50 in each condition) and plotted. P, significance by t test. (G) The signal intensity of foci was measured during entire lifespan. Representative data are displayed. A.U., arbitrary unit. (H) Consecutive images that were used for the analysis in G. The foci in the circle were analyzed. Phases where cells with the foci belong are indicated on the top.

ATAD5 knockdown generates inactive replication factories during S phase

The retention of DNA synthesis–deficient PCNA foci on the chromatin at the G2 phase and the prolonged duration of S phase in ATAD5 knockdown cells led us to investigate the staining pattern of PCNA and BrdU in S-phase cells. After a short pulse labeling with BrdU (3 min), control cells showed colocalization of BrdU and PCNA in all active replication foci. In contrast, a significant fraction (~7.5%) of S-phase cells showed a defective BrdU signal (ranging from weak to no detection) at PCNA foci in ATAD5 knockdown cells (Fig. 4, A and B). There were two types of PCNA foci in cells having a defective BrdU signal: foci that colocalized with the attenuated BrdU signal (Fig. 4 A, yellow foci marked with an arrowhead) and foci without the BrdU signal (red foci marked with an arrow). These foci might represent sub-active and inactive replication factories, respectively. Cells having both types of foci were observed more frequently in the late S phase. Albeit less frequently, the former type of PCNA foci (having an attenuated BrdU signal) was more dominantly observed in the early S phase. A similar result was observed in the RPE cell (Fig. S3).

When cells were labeled with BrdU for a longer period of time (10 min), the percentage of cells with a defective BrdU signal at PCNA foci decreased to ~4% in ATAD5 knockdown cells (Fig. 4, B and C). After 10 min labeling with BrdU, the PCNA signal began to separate from the BrdU foci (Fig. 4 C, si-Ctrl cells), reflecting a local movement of nascent DNA at active replication factories (Sporbert et al., 2002). In contrast, many PCNA foci in ATAD5 knockdown cells remained colocalized with weak BrdU foci not separated from BrdU foci, indicating that the PCNA foci with attenuated BrdU signal are not active replication sites.

We examined the presence of CAF-1 at the PCNA foci with a defective BrdU signal by ATAD5 knockdown. CAF-1 colocalized with PCNA foci independent of the intensity of BrdU signal (Fig. 4 D). This suggests that replication factories remain on the chromatin after completion of DNA synthesis (inactive replication factory) or until DNA synthesis is almost complete (sub-active replication factory) in ATAD5 knockdown cells. Most ATAD5 knockdown cells with PCNA foci having a defective BrdU signal were in late S phase or G2 phase with a small portion in early S phase (Fig. 4 E). Collectively,

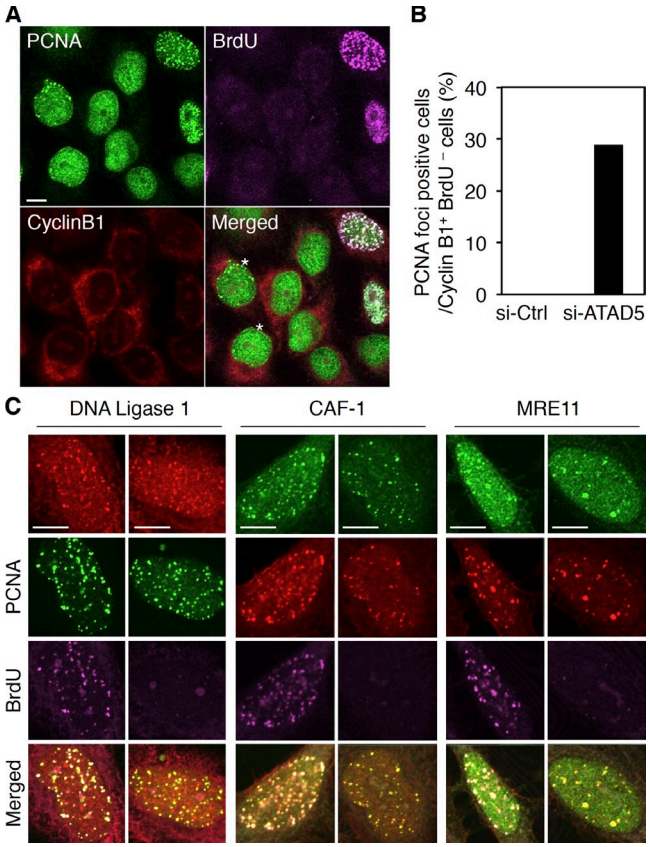

Figure 3. **ATAD5 knockdown retains inactive replication factories at the G2 phase.** 72 h after transfection of *ATAD5* or control siRNAs, HeLa cells were pulse-labeled with BrdU for 3 min, fixed, stained with anti-PCNA, anti-BrdU, and anti-cyclin B1 antibodies, and analyzed by confocal microscopy. (A) Representative images from ATAD5 knockdown cells. An asterisk indicates a cyclin B1–positive and BrdU-negative cell with PCNA foci. (B) The percentage of cells with PCNA foci in cyclin B1–positive and BrdU-negative cells (n = 110 for si-Ctrl cells; n = 97 for si-ATAD5 cells from a single experiment) was calculated. (C) Cells knocked down for ATAD5 were pulse-labeled with BrdU for 3 min, fixed, stained with anti-PCNA, anti-BrdU and the indicated antibodies, and analyzed by confocal microscopy. Bars, 5 µm.

ATAD5 knockdown generates inactive replication factories in both S and G2 phases, which result in the prolonged lifespan of PCNA foci.

Reduced expression of ATAD5 results in PCNA accumulation on the chromatin

Because PCNA accumulates at replication foci with an extended lifespan in ATAD5 knockdown cells, we predicted that the levels of chromatin-bound PCNA would increase as well. As expected, PCNA accumulated on the chromatin without changing its overall level when ATAD5 was depleted in HEK293T and HeLa cells (Fig. 5, A and B). Similar results were observed using a yeast *elg1*-deficient strain in control experiments (Parnas et al., 2010; Kubota et al., 2011). PCNA ubiquitylation was also increased after ATAD5 knockdown, as we previously reported (Lee et al., 2010). The chromatin-bound PCNA level showed a positive correlation with the knockdown efficiency of different siRNAs (Fig. 5 A). Reciprocal reduction of soluble PCNA level was evident by ATAD5 knockdown (Fig. 5 B), which corresponded to the maintenance of overall PCNA level. Expression of ATAD5 resistant to siRNA knockdown under the same conditions restored chromatin-bound PCNA level comparable to control siRNA, ruling out off-target effects (Fig. 5 C).

As PCNA functions as a platform for other replisome proteins (Sporbert et al., 2005), we speculated increased chromatin-bound level of other replication proteins after ATAD5 knockdown. In fact, the levels of many replication proteins were increased on the chromatin in ATAD5 knockdown cells (Fig. 5 D), which includes FEN1 and DNA ligase 1 protein, which are essential for Okazaki fragment maturation, MSH2, a mismatch repair protein, and MRE11. This might be partly explained by the retention of those proteins in the sub-active and/or inactive replication factories (Figs. 3 C and 4 D). Contrary to what is expected from the immunostaining data (Figs. 3 C and 4 D), the chromatin-bound level of CAF-1 was not changed after ATAD5 knockdown. This could be the result of the cross-linking step during the slide preparation for confocal microscopy, which allows for the detection of a weak association of CAF-1 with PCNA. The simultaneous knockdown of PCNA and ATAD5 reduced the chromatin accumulation of all replication proteins tested (Fig. 5 E), suggesting a PCNA-dependent retention of these replication proteins on the chromatin.

Eukaryotic cells have two RLCs besides ATAD5–RLC: RAD17–RLC and CTF18–RLC (Green et al., 2000; Mayer et al., 2001). We did not observe any difference in chromatin-bound PCNA level upon knockdown of RAD17 or CTF18 (Fig. 5 F). Collectively, the level of chromatin-bound PCNA is specifically affected by ATAD5 protein level.

Ectopic ATAD5 expression reduces PCNA on the chromatin

To understand the regulation mechanism of chromatin-bound PCNA by ATAD5, we examined the localization of ATAD5 in a cell line that stably expresses FLAG-tagged ATAD5. ATAD5 completely colocalized with PCNA at replication foci (Fig. 6 A), classifying ATAD5 as a replisome protein.

To investigate whether ATAD5 could unload PCNA from chromatin, we checked chromatin-bound PCNA level when ATAD5 protein was overexpressed. ATAD5 overexpression alone did not affect the PCNA level on the chromatin. However, knockdown of RFC1 with ATAD5 overexpression reduced chromatin-bound PCNA level (Fig. 6 B). This suggested that the available amount of small RFC subunits could be the limiting factor on the chromatin PCNA level. However, when small RFC subunits were coexpressed with ATAD5, we could not observe the reduction of the chromatin-bound PCNA level (unpublished data). This result rules out our interpretation of Fig. 6 B that small RFC subunits are the limiting factor. An alternative explanation could be that the balance of active replication site occupancy between RFC and ATAD5–RLC might be important for regulating chromatin-bound PCNA level. Enhancement of RFC1 knockdown by using more siRNA decreased PCNA level on the chromatin (Fig. 6 C). However, even under this condition, simultaneous knockdowns of ATAD5 restored the level of chromatin-bound PCNA similar to the level of ATAD5 knockdown alone (Fig. 6 C), suggesting that the increase of the chromatin-bound

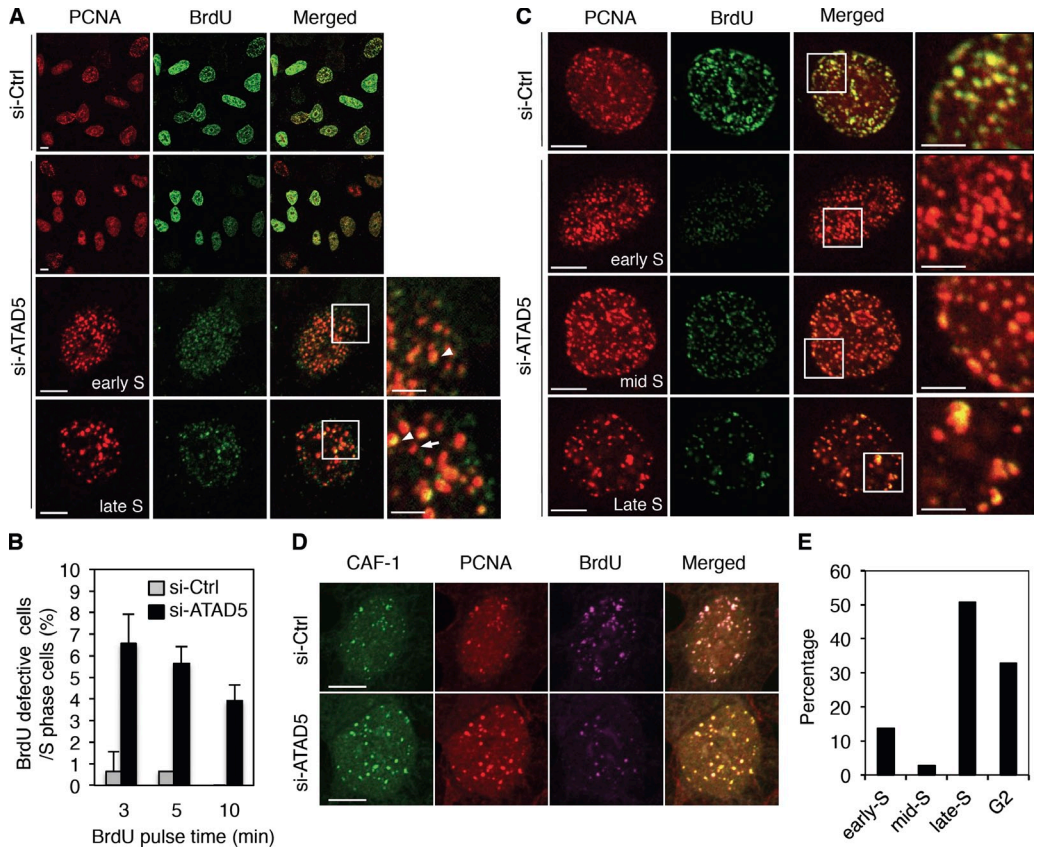

Figure 4. **ATAD5 knockdown generates inactive replication factories during S phase.** 72 h after transfection of *ATAD5* or control siRNAs, HeLa cells were pulse-labeled with BrdU for 3 (A, B, D, and E), 5 (B), or 10 min (B and C), fixed, stained with anti-PCNA and anti-BrdU or anti–CAF-1 antibodies, and analyzed by confocal microscopy. (A and C) The region in the inner squares is magnified and displayed to the right with a bar corresponding to 2 µm. Arrow, BrdU signal-null replication factories; arrowhead, replication factories with BrdU signal. (B) The percentage of cells in S phase with BrdU signal-defective PCNA foci was calculated from at least two independent experiments at each BrdU pulse-labeling time point and mean values were calculated. Error bars indicate SD. (D) Representative images from triple staining with anti-PCNA, anti-BrdU, and anti–CAF-1 antibodies. (E) Cells with BrdU signal-defective PCNA foci (n = 73 from multiple experiments) were classified based on the categories set in Fig. 2 A and the percentage was displayed. Bars (all images): 5 µm.

PCNA in ATAD5 knockdown cells appeared to result from defects in unloading of PCNA rather than acceleration in loading of PCNA by RFC1. However, we still cannot exclude the possibility that ATAD5 functions as an inhibitor of PCNA loading.

PCNA is spontaneously ubiquitylated in nondamaged cells or when replication forks are stalled by exogenous stresses (Fox et al., 2011). Because ATAD5 depletion increases PCNA ubiquitylation in both human and mouse (Lee et al., 2010; Bell et al., 2011), we investigated whether the presence of ubiquitylated PCNA (PCNA-Ub), or the condition that enhances PCNA-Ub, could also affect the level of PCNA on the chromatin. PCNA-Ub induced by UV irradiation did not affect the level of chromatin-bound PCNA (Fig. 6 D). Furthermore, the level of chromatin-bound PCNA in ATAD5 knockdown cells was not further increased by UV irradiation despite a synergistic increase in PCNA-Ub. Furthermore, the ectopic expression of ATAD5 mutant protein (ATAD5 UAF1del) that does not interact with the USP1–UAF1 complex and results in defective PCNA deubiquitylation (Lee et al., 2010; Yang et al., 2011) reduced chromatin-bound PCNA level similar to the ectopic expression of wild-type ATAD5 (Fig. 6 E). The ectopic expression of ATAD5 UAF1del mutant removed PCNA-Ub from the chromatin-bound protein fractions. Previously, we showed that the expression of the same mutant could not reduce the level of PCNA-Ub in the nuclear extract (Lee et al., 2010; Yang et al., 2011). It suggests that ATAD5 UAF1del mutant protein has PCNA-unloading activity even though it is defective in recruitment of the USP1–UAF1 complex to PCNA-Ub to remove ubiquitin from PCNA. Taken together, increased level of PCNA-Ub does not explain the enhanced level of PCNA on the chromatin after ATAD5 knockdown, irrespective of whether the source of PCNA-Ub is replication stalling or dysregulation of USP1 activity.

ATAD5 knockdown slows DNA replication rate

The presence of inactive replication factories might affect DNA replication in ATAD5 knockdown cells. To investigate changes in DNA replication rate by ATAD5 knockdown, we measured the incorporation of a thymidine analogue, ethynyl deoxyuridine (EdU), into replicating DNA. Microscopic data show that EdU incorporation was reduced in ATAD5 knockdown compared with control for all conditions tested (Fig. 7 A). The difference between the two cells became larger with longer incubation

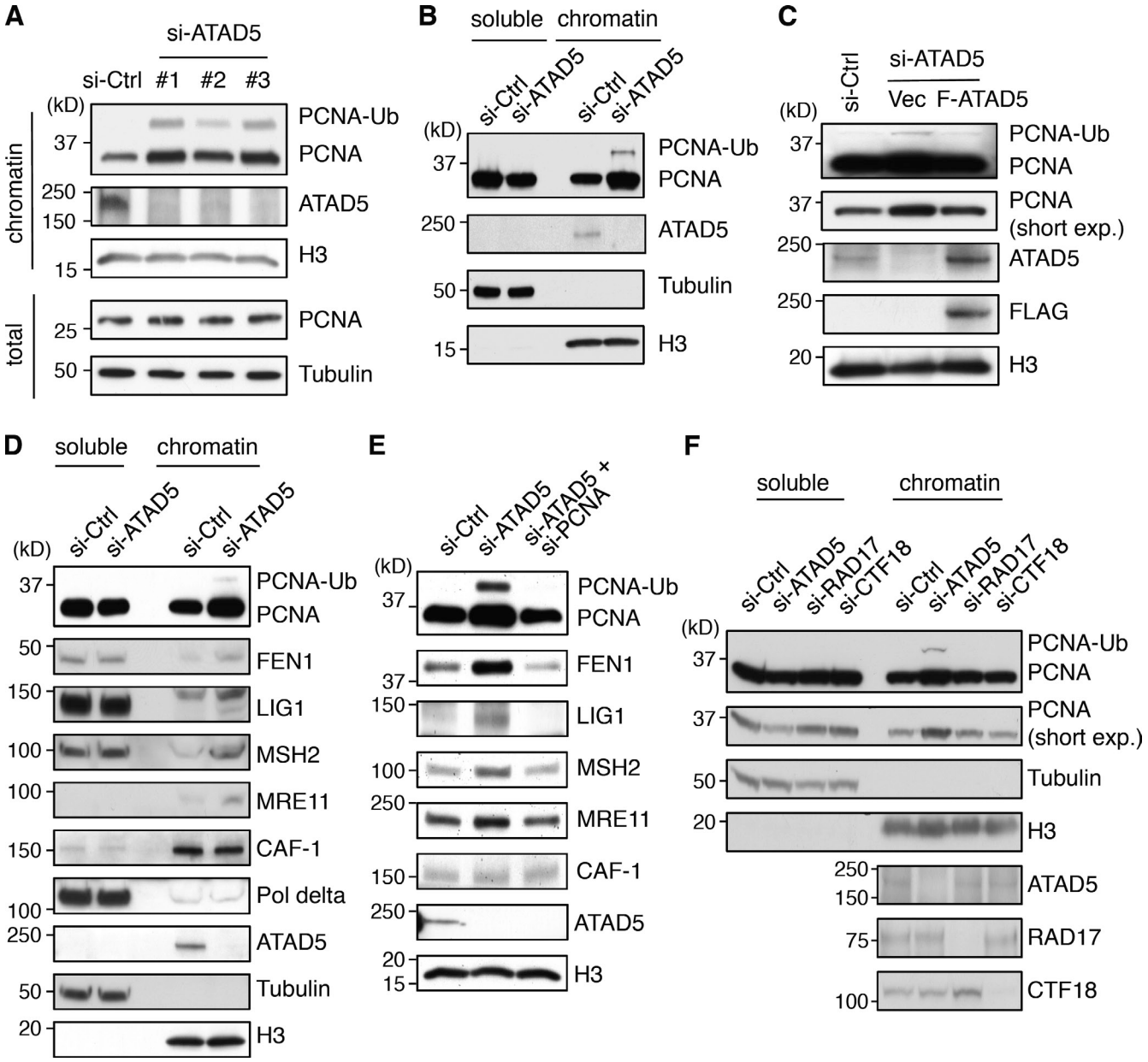

Figure 5. **ATAD5 knockdown accumulates replication proteins on the chromatin in a PCNA-dependent manner.** In all experiments, cells were transfected with *ATAD5* or control siRNAs and protein level was detected in Triton X-100 soluble (soluble) or insoluble (chromatin-bound) proteins. (A, C, and F) HEK293T cells. (B, D, and E) HeLa cells. (B–F) *ATAD5* siRNA #3 in A was used. (C) Cells were cotransfected with a combination of *ATAD5* siRNA and DNA vector expressing FLAG-tagged ATAD5 (F-ATAD5) or empty vector (Vec). Chromatin-bound proteins were isolated for immunoblot assay. (E) Cells were transfected with a combination of *ATAD5* or *PCNA* siRNAs. Chromatin-bound proteins were isolated for immunoblot assay. (F) Cells were transfected with siRNAs targeting *ATAD5*, *RAD17*, or *CTF18*. Tubulin and histone H3 (H3) were used as loading controls for total lysates or soluble fractions, and chromatin-bound fractions, respectively. Short exp; short exposure.

time with EdU (Fig. 7, B and C), suggesting that replication defect by ATAD5 knockdown accumulates. These data indicate that the overall DNA replication rate is slower in ATAD5 knockdown compared with control. It was consistent in the flow cytometry analysis. Similar to the BrdU incorporation, the percentage of EdU-positive cells was increased by ATAD5 knockdown compared with the control (Fig. 7 D). The intensity of EdU-positive peak shifted to the left, representing a lower EdU signal in ATAD5 knockdown cells. The extent of DNA synthesis measured by EdU intensity in EdU-positive cells was 40% less in ATAD5 knockdown cells than control cells (Fig. 7 E). In addition, shifting of the entire peak indicates that the reduction in replication rate occurred in the majority of the cell population after ATAD5 knockdown.

The overall replication rate can be affected by replication fork velocity and the number of replication origins fired. To determine the cause of the reduced replication rate after ATAD5 knockdown, we measured the fork velocity (Fig. 7 F) and distance between replication origins (Fig. 7 G) by DNA combing assay. The latter can indirectly determine the number

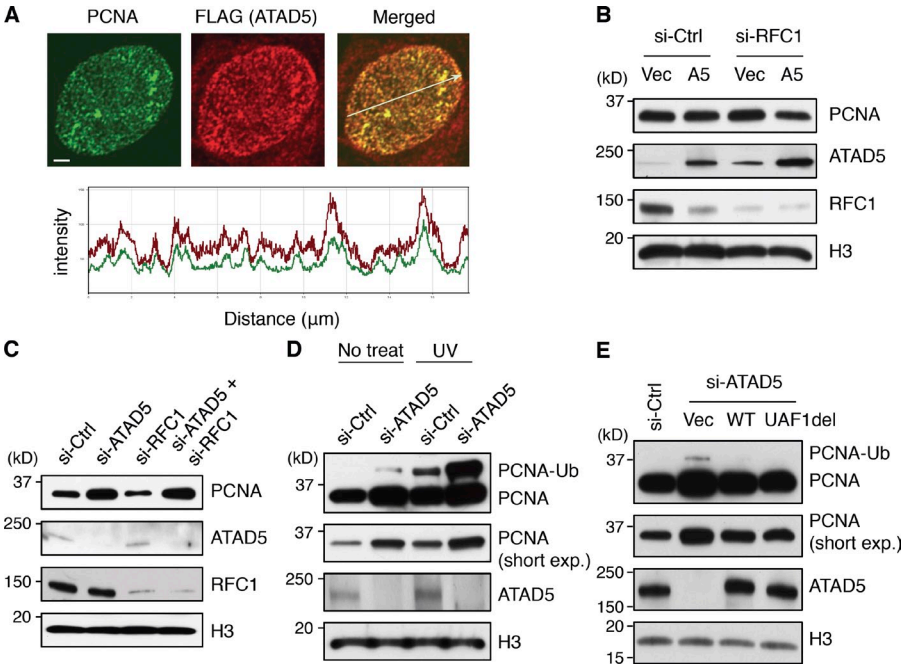

Figure 6. **ATAD5 removes PCNA from the chromatin in replication factories.** (A) RPE cells stably expressing FLAG-tagged ATAD5 protein were fixed, stained with anti-PCNA and anti-FLAG antibodies, and analyzed by confocal microscopy. The histogram at the bottom indicates colocalization of PCNA (green) and FLAG-ATAD5 (red) signal intensities following the line in the merged image. Bars, 2 μm. (B–E) 72 h after transfection, chromatin-bound proteins were isolated for immunoblot assay. (B) HEK293T cells were cotransfected with a combination of *RFC1* siRNA and a plasmid expressing ATAD5 protein (A5) or empty vector (Vec). (C) HeLa cells were transfected with a combination of *ATAD5* or *RFC1* siRNAs with the ratio of 1:5. (D) HeLa cells were irradiated with 60 J/m^2 UV at 72 h after transfection and incubated for another 12 h. (E) HEK293T cells were cotransfected with a combination of *ATAD5* siRNA and a plasmid expressing wild-type (WT) or mutant (UAF1del) ATAD5. Histone H3 (H3) was used as loading controls for chromatin-bound fractions. Short exp, short exposure.

of fired replication origins. Unexpectedly, there was no reduction in both fork velocity (1.601 kb/min for si-Ctrl vs. 1.751 kb/min for si-ATAD5) and inter-origin distances in ATAD5 knockdown compared with control. These results suggest that there seems to be another reason for the slow replication rate by ATAD5 knockdown.

ATAD5 knockdown results in S-phase delay

Consistent with the reduced replication rate, we observed the accumulation of S-phase cells after ATAD5 knockdown in three different cell lines (Fig. 8 A). Detailed analysis of cell cycle progression showed that progression through S phase was

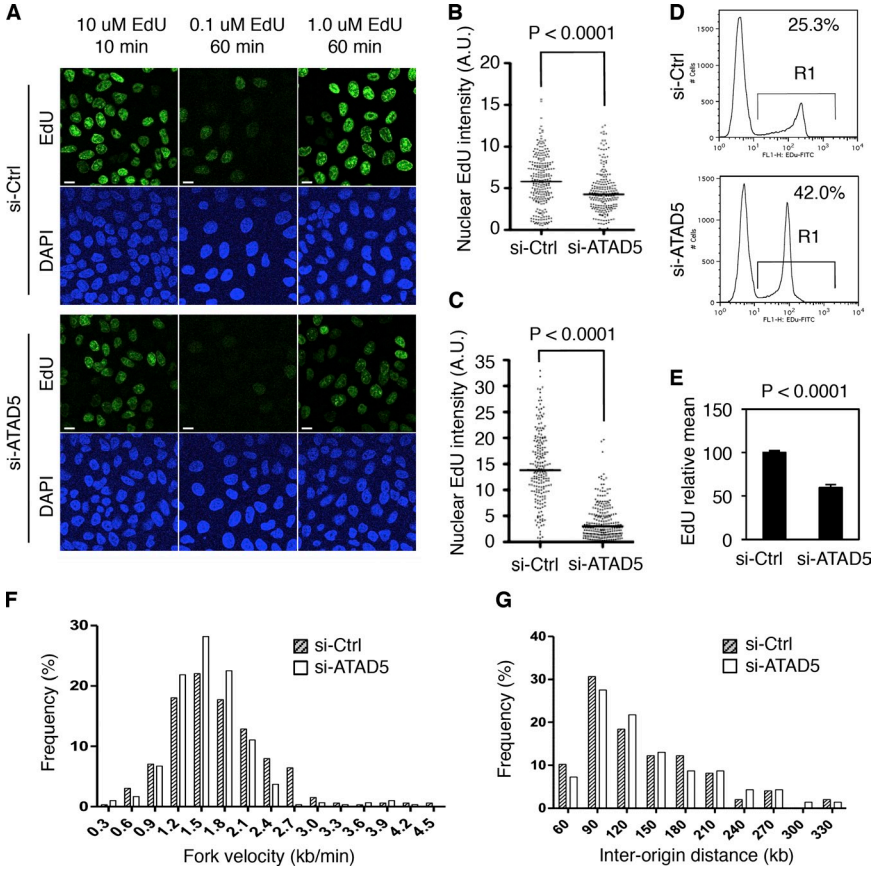

Figure 7. **ATAD5 knockdown slows DNA replication rate.** In all experiments, HeLa cells were analyzed 72 h after transfection of *ATAD5* or control siRNAs. (A) Cells were pulse-labeled with EdU as indicated and fixed for microscopic analysis. Bars, 10 μm. (B and C) Box blots showing the quantitation of nuclear EdU intensity. $n > 200$ in each condition from a single experiment; 10 μM EdU for 10 min (B), 1 μM EdU for 1 h (C). A.U., arbitrary unit; Bar in the graph, median value. (D) Cells were pulse-labeled with 10 μM EdU for 1 h, fixed, and permeabilized for flow cytometry analysis. The data shown are from a single representative experiment out of three repeats. Numbers are the mean percentage of EdU-positive cells (R1). (E) The EdU geometric mean intensity of R1 area in D was obtained from three independent experiments and mean values were calculated. Error bars indicate SD. (F and G) Cells were subjected to the DNA combing assay. The data shown are from a single representative experiment out of three repeats. (F) The distribution of the replication fork velocity was calculated ($n = 298$ for si-Ctrl cells; $n = 327$ for si-ATAD5 cells). (G) The distribution of the inter-origin distances was determined by measuring the distance between two identified replication initiation origins. P, significance by *t* test.

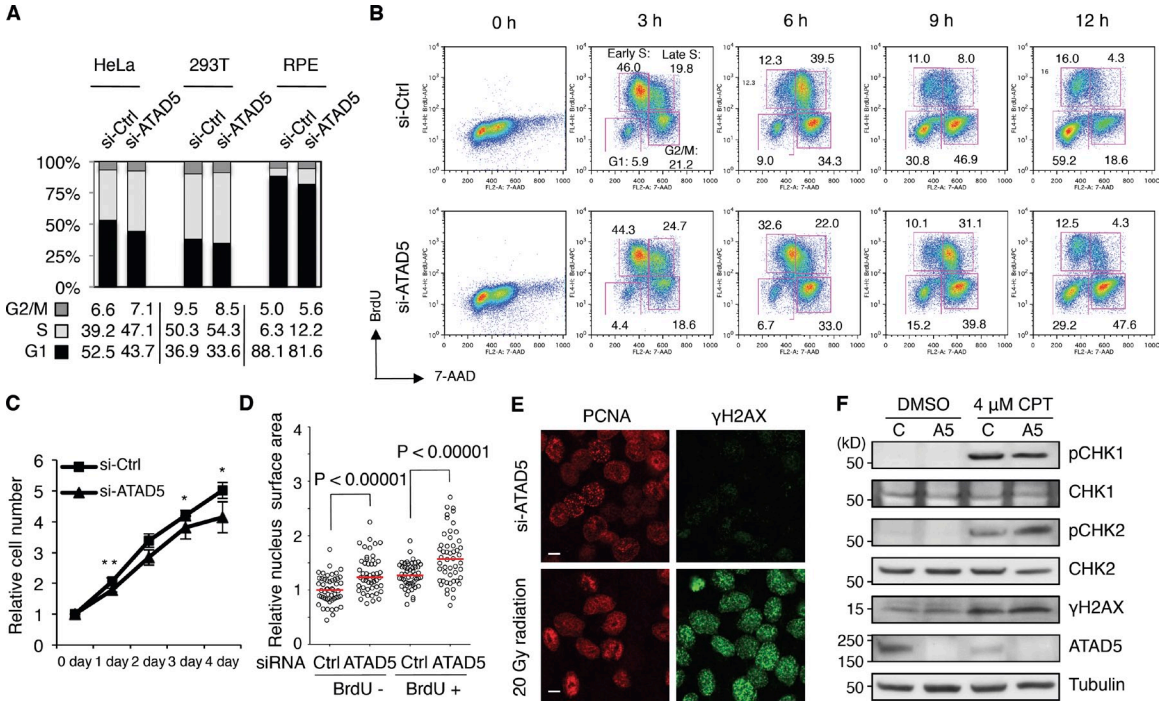

Figure 8. **ATAD5 knockdown delays S-phase cell cycle progression.** In all experiments, HeLa cells were analyzed 72 h after transfection of *ATAD5* or control siRNAs unless otherwise specified. (A) Cell cycle was measured by flow cytometry. The relative percentage of cell cycle stages was calculated from three independent experiments and displayed as a graph with the mean value below. (B) 48 h after transfection, cells were arrested with a double thymidine block. At indicated times after release from the G1/S block, cells were pulse-labeled with BrdU for 30 min and collected for cell cycle analysis. The data shown are from a single representative experiment out of two repeats. Numbers are the relative percentage of cell cycle stage. Early and late S phases indicate 7-AAD low and high cells, respectively. (C) Cell numbers were colorimetrically measured. **, $P < 0.05$; *, $P < 0.01$, by *t* test. Error bars indicate SD. (D) Cells were pulse-labeled with BrdU for 10 min, fixed, stained with anti-BrdU antibody, mounted with DAPI reagent, and analyzed by confocal microscopy. Relative nuclear surface size ($n = 50$ in each condition from a single experiment) was calculated. Red bars in the graph, median value; P, significance by *t* test. (E) Cells were treated with 20 gray (Gy) of γ-radiation, incubated for 30 min, fixed, and stained with both anti-PCNA and anti-γH2AX antibodies and analyzed by confocal microscopy. Bar, 5 μm. (F) Cells were treated with 4 μM CPT for 1 h and total extracts were isolated for immunoblot assay.

significantly delayed in ATAD5 knockdown cells after releasing from the G1/S arrest by a double thymidine block (Fig. 8 B). The difference between ATAD5 knockdown and control cells was evident as early as 6 h and was exacerbated at later time points. Specifically, the majority of control cells had transitioned to the G2/M phase at 9 h, whereas 41.2% of ATAD5 knockdown cells still remained in S phase. A similar result was observed in the HEK 293T cell line (Fig. S4). In addition, ATAD5 knockdown reduced proliferation compared with control cells (Fig. 8 C). These results are consistent with observations in a yeast *elg1*-deficient strain (Bellaoui et al., 2003; Kanellis et al., 2003). Thus, ATAD5 knockdown delays progression of the S phase of the cell cycle, which might result from defects in DNA replication.

We observed that ATAD5 knockdown cells appear to be larger than control cells in their cellular and nuclear size (Fig. 1 A). The increase in cell size after ATAD5 knockdown was confirmed by flow cytometry analysis (Fig. S5 A). It was not the result of an siRNA off-target effect because normal cell size was restored upon the expression of knockdown-resistant ATAD5 (Fig. S5 B). When the surface size of the nucleus was measured from multiple microscopic images, both BrdU-positive and -negative cells displayed significantly larger nuclear sizes upon ATAD5 knockdown (Fig. 8 D), suggesting that the enlarged nuclei in ATAD5 knockdown cells are present both in S phase and non-S phase cells. Because the regulation of cell size is closely related to doubling time and cell cycle progression (Padte et al., 2006), the enlarged cell size after ATAD5 knockdown correlates well with changes in cell cycle profile and proliferation rate (Fig. 8, A and C).

S-phase progression can be delayed by activation of the intra-S checkpoint. Spontaneous DNA damage was observed in human cells with prolonged ATAD5 depletion by short hairpin RNA (Sikdar et al., 2009). Thus, we investigated whether siRNA-mediated transient ATAD5 knockdown could induce DNA damage. In contrast to a clear induction of γH2AX, a marker for DNA damage, by treatment with 20 Gy of γ-radiation or 4 μM camptothecin (CPT), there was no detectable induction of γH2AX foci or increase in the level of γH2AX in ATAD5 knockdown cells (Fig. 8, E and F). Similarly, we could not detect any checkpoint activation, as determined by CHK1 and CHK2 phosphorylation, after ATAD5 knockdown (Fig. 8 F). In addition, ATAD5 knockdown did not show any additive effect in γH2AX level or CHK1 and CHK2 phosphorylation after CPT treatment. All these data indicate that transient ATAD5 knockdown does not induce DNA damage and checkpoint activation.

ATAD5 ATPase domain is important for proper function in replication factory

ATAD5 protein has an ATPase domain. Amino acid sequences at the ATPase domain are well conserved among RFC proteins as well as RLC proteins throughout evolution (Fig. 9 A). This is especially true for the lysine (K) residue, which is conserved in

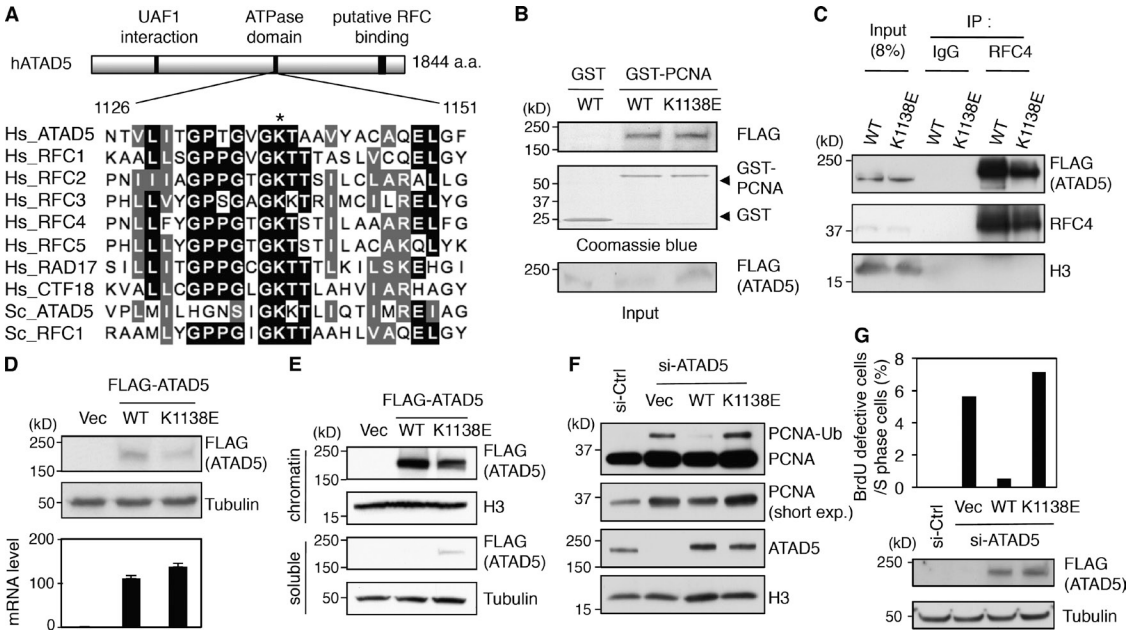

Figure 9. **ATAD5 ATPase domain is important for removal of PCNA from chromatin.** (A) Peptide sequence alignment for the ATPase domains of RFC proteins. Hs, *Homo sapiens*; Sc, *Saccharomyces cerevisiae*. An asterisk indicates a conserved lysine (K) residue. (B) GST or GST-PCNA proteins were mixed with protein extracts containing ATAD5 wild-type (WT) or K1138E mutant proteins, pulled down and then subjected to immunoblot assay. (C) HEK293T cells were transfected with a preadjusted amount of plasmid DNA to express same amount of ATAD5 wild-type or K1138E mutant proteins. After 48 h, chromatin-bound proteins were isolated for immunoprecipitation. (D) HEK293T cells were transfected with the same amount of plasmid DNA expressing ATAD5 wild-type or K1138E mutant proteins. After 48 h, total proteins and RNA were isolated for immunoblot assay (top) and quantitative RT-PCR analysis (bottom), respectively. The ATAD5 transcript levels were corrected by normalizing them to the transcript levels of *β-actin*. (E) HEK293T cells were transfected with a preadjusted amount of plasmid DNA to express the same amount of ATAD5 wild-type or K1138E mutant proteins. After 48 h, soluble and chromatin-bound proteins were isolated for immunoblot assay. (F) HEK293T cells were transfected with a combination of *ATAD5* siRNA and a preadjusted amount of plasmid DNA to express the same amount of ATAD5 wild-type or K1138E mutant proteins on the chromatin. After 72 h, chromatin-bound proteins were isolated for immunoblot assay. (G) HeLa cells were transfected with a combination of *ATAD5* siRNA and a plasmid expressing ATAD5 wild-type or K1138E mutant protein. After 72 h, cells were pulse-labeled with BrdU for 3 min, fixed, and stained with both anti-PCNA and anti-BrdU antibodies and analyzed by confocal microscopy. The percentage of BrdU-weak cells in S phase was calculated. $n > 300$ in each case from a single experiment. A portion of cells was used for immunoblot assay.

all ATPase domains. Mutation of this critical K residue to glutamate (E) in RFC1, RFC2, RFC3, or RFC4 impairs the ATPase as well as the replicative activities of the canonical RFC complex without affecting complex assembly in both yeast and human (Cai et al., 1998; Schmidt et al., 2001). Based on the protein alignment data (Fig. 9 A), we generated a putative ATAD5 ATPase mutant by changing K1138 residue to E (K1138E).

The ATAD5 K1138E mutant protein interacted with PCNA as well as RFC4, although the binding affinity to RFC4 was slightly weaker than wild-type ATAD5 (Fig. 9, B and C, respectively). Despite similar transcript levels, the ATAD5 K1138E mutant protein was present at lower levels than wild-type ATAD5 protein, suggesting the ATAD5 K1138E mutation caused protein instability (Fig. 9 D). When a comparable level of ATAD5 K1138E expression was achieved by transfecting more expression plasmid, we found that chromatin retention of the ATAD5 K1138E protein was also slightly defective, resulting in a significant amount of the mutant protein in the soluble fraction (Fig. 9 E). The defect in chromatin retention could be one of the reasons for protein instability.

Lastly, we investigated whether the ATAD5 K1138E protein could reduce the level of chromatin-bound PCNA similar to the wild-type protein. Unlike wild-type ATAD5, the expression of siRNA-resistant ATAD5 K1138E mutant protein in ATAD5 knockdown cells did not restore PCNA level on the chromatin (Fig. 9 F). We also examined the effect of the ATAD5 K1138E mutation on the performance of the replication factories. In contrast to the wild-type protein, expression of the ATAD5 K1138E mutant protein did not reduce the percentage of cells having defective replication factories with a defective BrdU signal (Fig. 9 G). Taken together, these results indicate that the ATAD5 ATPase domain is important for proper ATAD5 function in replication factories.

Discussion

In this study, we demonstrated that ATAD5 regulates the lifespan of replication factories. ATAD5 knockdown caused accumulation of PCNA in the replication factories (Figs. 1, 4, and 5). Enlargement and prolonged duration of PCNA foci in ATAD5 knockdown cells (Figs. 1 and 2 F) strongly suggest that ATAD5 functions to unload PCNA at the replication factories. Because other replication proteins remained in inactive replication factories after ATAD5 knockdown (Figs. 3 C and 4 D) and their retention on the chromatin was dependent on chromatin-bound PCNA (Fig. 5), disassembly of replication factories appears to be closely related to PCNA unloading. The requirement of intact ATPase domain of ATAD5 for the regulation of chromatin-bound

PCNA levels (Fig. 9 F) and dismantlement of replication factories (Fig. 9 G) suggest ATAD5–RLC's active role in unloading PCNA to facilitate these processes. The majority of replication factories having defective BrdU signal were observed in late S and G2 phases after ATAD5 knockdown (Fig. 4 E), suggesting that ATAD5–RLC functions to disassemble replication factories when replication factories complete their function. Therefore, defective ATAD5–RLC causes BrdU-negative or attenuated replication factories to remain on the chromatin and extend their lifespan.

The replication rate in ATAD5 knockdown cells was slow (Fig. 7). This could be a result from the inefficient performance of post-DNA synthesis process at replication factories. In both prokaryotes and eukaryotes, the presence of a stationary clamp reservoir with a rapid turnover of clamp proteins and the recruitment of replication proteins were microscopically observed (Sporbert et al., 2005; Su'etsugu and Errington, 2011). Highly accumulated proteins at inactive replication factories after ATAD5 knockdown (Figs. 4 D and 5 D) could delay specific sub-S phases, especially after DNA synthesis (Fig. 2 C), until those inactive replication factories are disassembled to release the replication proteins so that they could be recycled for completion of post-DNA synthesis process in other active replication factories. Consistently, depletion of CAF-1 delays the replication rate (Hoek and Stillman, 2003). Alternatively, ATAD5 might assist the replication machinery to replicate certain chromosomal locations efficiently that are difficult to replicate (Rothstein et al., 2000). Repetitive DNAs in many locations including centromeres are replicated throughout late S phase (Ten Hagen et al., 1990). Because most ATAD5 knockdown cells have inactive replication factories that are at the late S phase (Fig. 4 E), it is possible that ATAD5 might have unique roles for assisting the replication of such genomic locations. Such a possibility could explain the DNA combing result in terms of detection sensitivity. Under the labeling condition that we used in the DNA combing assay, the calculated detection limit of replication fork speed is 0.3 kb/min. It is possible that after ATAD5 knockdown, stretches of DNA synthesized near chromosomal locations that are difficult to replicate could be too short to be detected in the DNA combing assay.

ATAD5–RLC regulates the life cycle of replication factories by changing the level of PCNA in the replication factory. This could possibly occur by PCNA unloading. According to a previous report in budding yeast, Elg1–RLC has no PCNA loading/unloading activity in an in vitro system where the same activities of Ctf18–RLC were observed (Bylund and Burgers, 2005). However, indirect evidences, including our current results, implicate ATAD5–RLC in unloading PCNA. Specific increase in the level of chromatin-bound PCNA by ATAD5 knockdown supports this model (Fig. 5 F). In two recent reports, similar observations in yeast were briefly mentioned in their control experiments (Parnas et al., 2010; Kubota et al., 2011). There was even a slight reduction in the level of chromatin-bound PCNA in yeast *ctf18* mutants. Additionally, the inactivation of yeast Ctf18–RLC or overexpression of yeast Elg1p was synthetic lethal with the *rfc1-44* mutant, and the synthetic-lethal phenotype of *ctf18 rfc1* mutant was rescued by *elg1* mutation (Kim et al., 2005). These genetic interactions suggest that both Rfc1p and Ctf18p load PCNA, whereas Elg1p unloads PCNA. Lastly, yeast Elg1p physically and genetically interacts with Rad27p (a yeast homologue of FEN1), implicating ATAD5–RLC in PCNA unloading (Kanellis et al., 2003). It should be stressed that all replication factories ultimately complete their cycle, even in ATAD5 knockdown cells. It is possible that PCNA could be unloaded redundantly by two other clamp loaders, RFC or CTF18–RLC in the absence of ATAD5–RLC. However, the prolonged ATAD5 deficiency in rapidly proliferating cells during embryonic development could not be complemented by other clamps. This could be the reason why the homozygous null mutation of *Atad5* caused the embryonic lethality in mice (Bell et al., 2011). Taking all these data together, we propose that ATAD5–RLC is a major complex for PCNA unloading.

We recently reported a tumor-suppressive function of ATAD5 in both mice and humans (Bell et al., 2011). Haploinsufficiency of Atad5 predisposed mice to develop tumors. Somatic mutations of the *ATAD5* gene were found in several endometrial tumors. We report here that ATAD5 has roles in DNA replication in addition to its role in DNA repair in response to DNA damage. Because homozygous *usp1*-null mice show neither embryonic lethality nor tumor predisposition, the dysregulation of PCNA ubiquitylation is not enough to explain the essential embryonic and tumor-suppressive functions of ATAD5. Rather, defects in DNA replication, including dysregulation of both cell cycle and replication factory cycle by ATAD5 knockdown observed in this study, could explain tumorigenesis as well as embryonic lethality of *Atad5*-null mice.

Materials and methods

Cell culture, reagents, and antibodies

Human embryonic kidney (HEK) 293T cells and HeLa cells were maintained in Dulbecco's modified Eagle's medium (DMEM) containing 10% fetal bovine serum (FBS; Hyclone), 100 U/ml penicillin G, and 100 µg/ml streptomycin. HeLa cells stably expressing GFP-fused PCNA and mCherry protein–fused H2B were maintained in a same condition with additional 1 µg/ml puromycin and 0.5 mg/ml G418. The immortalized normal retinal pigment epithelial (RPE) cells were maintained in DMEM/Ham's F12 containing 10% FBS (Hyclone), 100 U/ml penicillin G, and 100 µg/ml streptomycin. RPE cells stably expressing FLAG-tagged ATAD5 were maintained in a same condition with additional 0.5 mg/ml G418. The following antibodies were used: anti-PCNA (PC10), anti-CHK1, anti-CHK2, anti-FEN1, anti-RAD17, and anti-RFC4 antibodies (Santa Cruz Biotechnology, Inc.); anti-LIG1 and anti-CTF18, and anti–CHK1-S317 antibodies (Bethyl Laboratories, Inc.); anti-FLAG, anti-BrdU, anti-RFC1, anti-MSH2, anti-CAF1, anti-cyclin B1, and anti-tubulin antibodies (Abcam); anti-histone H3 antibody (EMD Millipore); anti-MRE11 and anti-γH2AX antibodies (Genetex); anti-RPA antibody (EMD Millipore); anti–CHK2-T68 antibody (Cell Signaling Technology); and anti-polymerase delta antibody (BD). The anti–human ATAD5 antibody was raised in rabbits using N-terminal 1–297 amino acid fragments (Lee et al., 2010).

DNA constructs and siRNAs

Plasmids expressing full-length wild-type ATAD5 (p3×FLAG-ATAD5) protein and expressing UAF1 interaction-defective ATAD5 protein (ATAD5–UAF1del), both of which were cloned in p3×FLAG-CMV10 expression vector (Sigma-Aldrich), were described previously (Sikdar et al., 2009; Lee et al., 2010). The site-directed mutagenesis to generate plasmid DNA for ATAD5 K1138E mutant proteins was performed using the QuikChange site-directed mutagenesis kit (Agilent Technologies) according to the manufacturer's instructions with p3×FLAG-ATAD5 as a template.

ON-TARGETplus NON-targeting pool (#D-001810) and ON-TARGETplus SMART pool siRNAs for *ATAD5* (#L-004738), *RFC1* (#L-009290),

CTF18 (#L-013915), *RAD17* (#L-003294), and *PCNA* (#L-003289) were purchased from Thermo Fisher Scientific. To target the 3′ untranslated region (UTR) of ATAD5, siRNAs with the following sense and antisense sequences were purchased from Thermo Fisher Scientific: 5′-GGAAGGUAGAGUUCAUUAAUU-3′ (sense) and 5′-UUCCUUCCAUCUCAAGUAAUU-3′ (antisense).

Transfections and RNA interference

Transfections of plasmid DNA and siRNAs, either synthetic duplexes or SMART pool (50–100 nM), were performed using Lipofectamine2000 (Invitrogen) and Oligofectamine (Invitrogen), respectively, according to the manufacturer's instructions. Transfected cells were further incubated for 72 h before for further analysis. In some experiments, wild-type or mutant ATAD5 was expressed in cells in which the endogenous ATAD5 was knocked down by siRNA targeting 3′UTR of *ATAD5*. In these experiments, plasmids expressing wild-type or mutant ATAD5 protein were transfected 24 h after siRNA transfection.

Colorimetrical measurement of cell numbers

At 48 h (0 d) after transfection, the same number of cells was seeded into each well of 96-well plates and incubated in a 37°C incubator. Cells were frozen in a deep freezer at the indicated times. Samples were prepared using the CyQUANT Cell Proliferation Assay kit (Invitrogen) according to the manufacturer's instructions. Fluorescence was measured using a Fluoroskan Ascent FL microreader (Thermo Fisher Scientific) with excitation at 485 nm and emission detection at 530 nm. Each cell number was normalized to the number of cells at d 0.

Microbeads attachment experiment

Control and ATAD5 knockdown cells were allowed to bind to two different sized Polybeads Carboxylate Microspheres (Polysciences, Inc.), 2 and 0.75 µm, respectively, for 6 h. Then, both cells bound to different beads were harvested and plated in a single slide chamber and incubated for another 18 h before fixation.

Confocal microscope sample preparation

Cells were plated in LabTek chamber slides (Thermo Fisher Scientific) and incubated for 1 d before fixation with 100% methanol at −20°C for 30 min or used directly for live-cell imaging. For the staining of chromatin-bound PCNA, cells were pretreated with 0.5% Triton X-100 for 2 min before fixation. For BrdU labeling, cells were incubated with 20 µM BrdU for the indicated times before fixation. The fixed cells were stained with single or combined primary antibodies for 1 h at room temperature (RT). After washes with 0.05% Triton X-100 in PBS three times, Alexa Fluor–conjugated secondary antibodies were added and incubated for 30 min. For BrdU detection, BrdU-labeled cells were fixed with 4% paraformaldehyde for 5 min after immunostaining to detect proteins together with BrdU. Cells were then treated with 4N HCl for 10 min at RT. After rinsing with PBS, cells were stained with rat anti-BrdU antibody and then with the Alexa Fluor–conjugated secondary antibody. Cells were mounted using Prolong Gold Antifade reagent (Invitrogen). Alexa Fluor 488–, Alexa Fluor 568–, and Alexa Fluor 633–conjugated secondary antibodies were purchased from Invitrogen.

Microscope image acquisition

Confocal images were acquired at room temperature using an LSM 510 NLO Meta system (Carl Zeiss) mounted on an inverted microscope (Axiovert 200M; Carl Zeiss) with an oil immersion Plan-Apochromat 63x/NA 1.4 DIC objective lens (Carl Zeiss). Excitation wavelengths of 488, 561, and 633 nm were used for detection of Alexa Fluor 488, 568, and 633, respectively. Fluorescent emissions were collected using photomultiplier tubes with a BP 500–550 nm IR blocked filter, a BP 575–615 nm IR blocked filter, and an LP 650-nm filter, respectively. All confocal images were acquired with a 512 × 512-pixel frame size. The acquired images were post-processed using Image-Pro Plus v7.0 software (Bethesda, MD). A custom macro was designed for image processing. This macro was used to calibrate and filter the signal based on a Gaussian distribution. Using this macro, images were also segmented to remove those with touching nuclei or nuclei touching the image border, and the nuclei were outlined using DAPI staining as the template and copied throughout the appropriate fluorophore channel. Nuclei were then counted and measurements of nuclear area (μm^2) and fluorescent intensity (mean and sum) were recorded.

Live-cell imaging

Cells grown on glass-bottom dishes (MatTek Corporation) were imaged in a 37°C chamber with a secondary internal chamber that delivered humidified 5% CO_2. Wide-field images were collected using a Yokogawa Spinning Disk system (Carl Zeiss) mounted on an inverted microscope (Axio Observer Z1; Carl Zeiss) with an oil immersion Plan-Apochromat 63x/NA 1.4 DIC lens. All images were acquired every 10 min for 26 h using an EMCCD camera (Evolve; Photometrics) with an exposure time of 312 ms per Z slice acquisition, 2 × 2 binning, and a 512 × 512-pixel imaging field. Z-stacks were collected (7 images per stack) with an excitation wavelength of 488 nm and an emission filter of 525/50. Images were post-processed using the AxioVision software package, v4.8 (Carl Zeiss).

EdU incorporation analysis

Cells were labeled with EdU under different conditions and harvested for microscopic or flow cytometry analysis. For microscopic analysis, samples were prepared using the Click-it EdU Alexa Fluor 488 imaging kit (Life Technologies) according to the manufacturer's instructions. Data were analyzed using Image-Pro Plus 7.0 software. For flow cytometry analysis, samples were prepared using the Click-it EdU flow cytometry assay kit (Life Technologies) according to the manufacturer's instructions and subjected to FACS analysis. Data were analyzed using FlowJo software (Tree Star).

BrdU incorporation and cell cycle analysis

Cells were labeled with 10 µM BrdU for 30 min and harvested. Samples for cell cycle analysis were prepared using the APC BrdU Flow kit (BD) according to the manufacturer's instructions and subjected to FACS analysis using a FACSCalibur Analytic Flow cytometer (BD). Data were analyzed using FlowJo software (Tree Star).

Cell synchronization using a double thymidine block

To synchronize cells at the G1/S boundary, 2 mM thymidine was added. After 19 h, cells were washed three times with fresh medium, released for 9 h, and incubated with 2 mM thymidine for an additional 16 h. Cells were then allowed to grow under normal conditions and harvested every 3 h after release. The cell cycle stage was monitored by flow cytometry.

DNA molecular combing analysis

DNA-combing analyses of replicating DNA were performed according to the methods described previously (Conti et al., 2001). In brief, cells were pulse-labeled with 20 µM IdU (Sigma-Aldrich) for 20 min followed by second labeling with 50 µM CldU (MP Biomedicals) for 20 min before analysis. Cells were embedded in low-melting point Agarose plugs and lysed with proteinase K lysis buffer at 50°C overnight. After Agarose was digested with β-Agarase (New England Biolabs, Inc.), DNA was combed onto silanized surfaces (Microsurfaces, Inc.) and detected with anti-IdU (BD), anti-CldU (Accurate Chemical), and anti–single-strand DNA (EMD Millipore) antibodies. Images were captured with Attovision software using an epifluorescence microscope (Pathway; BD) and the signals were measured using ImageJ software (open source from National Cancer Institute, NIH) with custom-made macros (Conti et al., 2010). The replication fork velocity was calculated from the length of CldU and IdU signals.

Immunoprecipitation and immunoblot analysis

Triton X-100–soluble (soluble fraction) and Triton X-100–insoluble fractions (chromatin-bound fraction) were isolated and subjected to immunoprecipitation or immunoblot analysis with the methods described previously (Lee et al., 2010). In brief, "soluble fraction" was isolated by incubating cells in buffer A (100 mM NaCl, 300 mM sucrose, 3 mM $MgCl_2$, 10 mM Pipes, pH 6.8, 1 mM EGTA, 0.2% Triton X-100, 100 µM $NaVO_4$, 50 mM NaF, and protease inhibitors [Roche]) for 5 min on ice followed by centrifugation. Then "chromatin-bound fraction" was isolated by resuspending the pellet in buffer B (50 mM Tris-HCl, pH 7.5, 150 mM NaCl, 5 mM EDTA, 1% Triton X-100, 0.1% SDS, 100 µM $NaVO_4$, 50 mM NaF, and protease inhibitors) for 10 min on ice followed by sonication and centrifugation.

Online supplemental material

Fig. S1 shows the generation of abnormally large PCNA foci in RPE cells and in cells prepared in a single slide chamber after control and ATAD5 knockdown. Fig. S2 shows consecutive images of a single GFP-PCNA–positive cell from control and ATAD5 knockdown. Fig. S3 shows generation of inactive replication factories after ATAD5 knockdown in RPE cells. Fig. S4 shows a delay in S-phase cell cycle progression after ATAD5 knockdown in HEK293T cells. Fig. S5 has flow cytometry data showing increased cellular size in ATAD5 knockdown cells. Online supplemental material is available at http://www.jcb.org/cgi/content/full/jcb.201206084/DC1.

We thank the former laboratory member S. Banerjee for making the initial expression construct of the ATAD5 K1138E mutant; S. Wincovitch (Cytogenetics and Microscopy core in NHGRI) for image analysis; Dr. Geurlich (Institute of

Biochemistry, Department of Biology, Zurich, Switzerland) for HeLa cells expressing GFP-PCNA; D. Bell (NHGRI), D. Bodine (NHGRI), M. Lichten (NCI), Y. Seo (KAIST), E.J. Choi (PAP), and members in the Myung laboratory for helpful discussions and comments on the manuscript. K. Myung especially thanks E. Cho.

This research was supported by the intramural Research Programs of the National Human Genome Research Institute to K. Myung, and of the National Cancer Institute to M.I. Aladjem.

Submitted: 19 June 2012
Accepted: 5 December 2012

References

Banerjee, S., and K. Myung. 2004. Increased genome instability and telomere length in the elg1-deficient *Saccharomyces cerevisiae* mutant are regulated by S-phase checkpoints. *Eukaryot. Cell*. 3:1557–1566. http://dx.doi.org/10.1128/EC.3.6.1557-1566.2004

Bell, D.W., N. Sikdar, K.Y. Lee, J.C. Price, R. Chatterjee, H.D. Park, J. Fox, M. Ishiai, M.L. Rudd, L.M. Pollock, et al; NISC Comparative Sequencing Program. 2011. Predisposition to cancer caused by genetic and functional defects of mammalian Atad5. *PLoS Genet.* 7:e1002245. http://dx.doi.org/10.1371/journal.pgen.1002245

Bellaoui, M., M. Chang, J. Ou, H. Xu, C. Boone, and G.W. Brown. 2003. Elg1 forms an alternative RFC complex important for DNA replication and genome integrity. *EMBO J.* 22:4304–4313. http://dx.doi.org/10.1093/emboj/cdg406

Ben-Aroya, S., A. Koren, B. Liefshitz, R. Steinlauf, and M. Kupiec. 2003. ELG1, a yeast gene required for genome stability, forms a complex related to replication factor C. *Proc. Natl. Acad. Sci. USA*. 100:9906–9911. http://dx.doi.org/10.1073/pnas.1633757100

Berezney, R., D.D. Dubey, and J.A. Huberman. 2000. Heterogeneity of eukaryotic replicons, replicon clusters, and replication foci. *Chromosoma*. 108:471–484. http://dx.doi.org/10.1007/s004120050399

Bravo, R., and H. Macdonald-Bravo. 1987. Existence of two populations of cyclin/proliferating cell nuclear antigen during the cell cycle: association with DNA replication sites. *J. Cell Biol.* 105:1549–1554. http://dx.doi.org/10.1083/jcb.105.4.1549

Bylund, G.O., and P.M. Burgers. 2005. Replication protein A-directed unloading of PCNA by the Ctf18 cohesion establishment complex. *Mol. Cell. Biol.* 25:5445–5455. http://dx.doi.org/10.1128/MCB.25.13.5445-5455.2005

Cai, J., F. Uhlmann, E. Gibbs, H. Flores-Rozas, C.G. Lee, B. Phillips, J. Finkelstein, N. Yao, M. O'Donnell, and J. Hurwitz. 1996. Reconstitution of human replication factor C from its five subunits in baculovirus-infected insect cells. *Proc. Natl. Acad. Sci. USA*. 93:12896–12901. http://dx.doi.org/10.1073/pnas.93.23.12896

Cai, J., N. Yao, E. Gibbs, J. Finkelstein, B. Phillips, M. O'Donnell, and J. Hurwitz. 1998. ATP hydrolysis catalyzed by human replication factor C requires participation of multiple subunits. *Proc. Natl. Acad. Sci. USA*. 95:11607–11612. http://dx.doi.org/10.1073/pnas.95.20.11607

Celis, J.E., and A. Celis. 1985. Cell cycle-dependent variations in the distribution of the nuclear protein cyclin proliferating cell nuclear antigen in cultured cells: subdivision of S phase. *Proc. Natl. Acad. Sci. USA*. 82:3262–3266. http://dx.doi.org/10.1073/pnas.82.10.3262

Conti, C., S. Caburet, C. Schurra, and A. Bensimon. 2001. Molecular combing. *Curr. Protoc. Cytom.* Chapter 8:Unit 8 10.

Conti, C., E. Leo, G.S. Eichler, O. Sordet, M.M. Martin, A. Fan, M.I. Aladjem, and Y. Pommier. 2010. Inhibition of histone deacetylase in cancer cells slows down replication forks, activates dormant origins, and induces DNA damage. *Cancer Res.* 70:4470–4480. http://dx.doi.org/10.1158/0008-5472.CAN-09-3028

Davies, A.A., D. Huttner, Y. Daigaku, S. Chen, and H.D. Ulrich. 2008. Activation of ubiquitin-dependent DNA damage bypass is mediated by replication protein a. *Mol. Cell*. 29:625–636. http://dx.doi.org/10.1016/j.molcel.2007.12.016

Fox, J.T., K.Y. Lee, and K. Myung. 2011. Dynamic regulation of PCNA ubiquitylation/deubiquitylation. *FEBS Lett.* 585:2780–2785. http://dx.doi.org/10.1016/j.febslet.2011.05.053

Green, C.M., H. Erdjument-Bromage, P. Tempst, and N.F. Lowndes. 2000. A novel Rad24 checkpoint protein complex closely related to replication factor C. *Curr. Biol.* 10:39–42. http://dx.doi.org/10.1016/S0960-9822(99)00263-8

Hoek, M., and B. Stillman. 2003. Chromatin assembly factor 1 is essential and couples chromatin assembly to DNA replication in vivo. *Proc. Natl. Acad. Sci. USA*. 100:12183–12188. http://dx.doi.org/10.1073/pnas.1635158100

Hozák, P., D.A. Jackson, and P.R. Cook. 1994. Replication factories and nuclear bodies: the ultrastructural characterization of replication sites during the cell cycle. *J. Cell Sci.* 107:2191–2202.

Huang, M.E., A.G. Rio, A. Nicolas, and R.D. Kolodner. 2003. A genomewide screen in *Saccharomyces cerevisiae* for genes that suppress the accumulation of mutations. *Proc. Natl. Acad. Sci. USA*. 100:11529–11534. http://dx.doi.org/10.1073/pnas.2035018100

Kanellis, P., R. Agyei, and D. Durocher. 2003. Elg1 forms an alternative PCNA-interacting RFC complex required to maintain genome stability. *Curr. Biol.* 13:1583–1595. http://dx.doi.org/10.1016/S0960-9822(03)00578-5

Kim, J., K. Robertson, K.J. Mylonas, F.C. Gray, I. Charapitsa, and S.A. MacNeill. 2005. Contrasting effects of Elg1-RFC and Ctf18-RFC inactivation in the absence of fully functional RFC in fission yeast. *Nucleic Acids Res.* 33:4078–4089. http://dx.doi.org/10.1093/nar/gki728

Kim, J.M., K. Parmar, M. Huang, D.M. Weinstock, C.A. Ruit, J.L. Kutok, and A.D. D'Andrea. 2009. Inactivation of murine Usp1 results in genomic instability and a Fanconi anemia phenotype. *Dev. Cell*. 16:314–320. http://dx.doi.org/10.1016/j.devcel.2009.01.001

Kubota, T., S.I. Hiraga, K. Yamada, A.I. Lamond, and A.D. Donaldson. 2011. Quantitative proteomic analysis of chromatin reveals that Ctf18 acts in the DNA replication checkpoint. *Mol. Cell Proteomics*. 10:M110.005561. http://dx.doi.org/10.1074/mcp.M110.005561

Lee, K.Y., K. Yang, M.A. Cohn, N. Sikdar, A.D. D'Andrea, and K. Myung. 2010. Human ELG1 regulates the level of ubiquitinated proliferating cell nuclear antigen (PCNA) through Its interactions with PCNA and USP1. *J. Biol. Chem.* 285:10362–10369. http://dx.doi.org/10.1074/jbc.M109.092544

Leonhardt, H., H.P. Rahn, P. Weinzierl, A. Sporbert, T. Cremer, D. Zink, and M.C. Cardoso. 2000. Dynamics of DNA replication factories in living cells. *J. Cell Biol.* 149:271–280. http://dx.doi.org/10.1083/jcb.149.2.271

Lindsey-Boltz, L.A., V.P. Bermudez, J. Hurwitz, and A. Sancar. 2001. Purification and characterization of human DNA damage checkpoint Rad complexes. *Proc. Natl. Acad. Sci. USA*. 98:11236–11241. http://dx.doi.org/10.1073/pnas.201373498

Majka, J., and P.M. Burgers. 2003. Yeast Rad17/Mec3/Ddc1: a sliding clamp for the DNA damage checkpoint. *Proc. Natl. Acad. Sci. USA*. 100:2249–2254. http://dx.doi.org/10.1073/pnas.0437148100

Majka, J., and P.M. Burgers. 2004. The PCNA-RFC families of DNA clamps and clamp loaders. *Prog. Nucleic Acid Res. Mol. Biol.* 78:227–260. http://dx.doi.org/10.1016/S0079-6603(04)78006-X

Mayer, M.L., S.P. Gygi, R. Aebersold, and P. Hieter. 2001. Identification of RFC(Ctf18p, Ctf8p, Dcc1p): an alternative RFC complex required for sister chromatid cohesion in *S. cerevisiae*. *Mol. Cell*. 7:959–970. http://dx.doi.org/10.1016/S1097-2765(01)00254-4

Merkle, C.J., L.M. Karnitz, J.T. Henry-Sánchez, and J. Chen. 2003. Cloning and characterization of hCTF18, hCTF8, and hDCC1. Human homologs of a *Saccharomyces cerevisiae* complex involved in sister chromatid cohesion establishment. *J. Biol. Chem.* 278:30051–30056. http://dx.doi.org/10.1074/jbc.M211591200

Moldovan, G.L., B. Pfander, and S. Jentsch. 2007. PCNA, the maestro of the replication fork. *Cell*. 129:665–679. http://dx.doi.org/10.1016/j.cell.2007.05.003

Nakayasu, H., and R. Berezney. 1989. Mapping replicational sites in the eucaryotic cell nucleus. *J. Cell Biol.* 108:1–11. http://dx.doi.org/10.1083/jcb.108.1.1

Navadgi-Patil, V.M., and P.M. Burgers. 2009. A tale of two tails: activation of DNA damage checkpoint kinase Mec1/ATR by the 9-1-1 clamp and by Dpb11/TopBP1. *DNA Repair (Amst.)*. 8:996–1003. http://dx.doi.org/10.1016/j.dnarep.2009.03.011

Padte, N.N., S.G. Martin, M. Howard, and F. Chang. 2006. The cell-end factor pom1p inhibits mid1p in specification of the cell division plane in fission yeast. *Curr. Biol.* 16:2480–2487. http://dx.doi.org/10.1016/j.cub.2006.11.024

Parnas, O., A. Zipin-Roitman, B. Pfander, B. Liefshitz, Y. Mazor, S. Ben-Aroya, S. Jentsch, and M. Kupiec. 2010. Elg1, an alternative subunit of the RFC clamp loader, preferentially interacts with SUMOylated PCNA. *EMBO J.* 29:2611–2622. http://dx.doi.org/10.1038/emboj.2010.128

Pines, J., and T. Hunter. 1989. Isolation of a human cyclin cDNA: evidence for cyclin mRNA and protein regulation in the cell cycle and for interaction with p34cdc2. *Cell*. 58:833–846. http://dx.doi.org/10.1016/0092-8674(89)90936-7

Rothstein, R., B. Michel, and S. Gangloff. 2000. Replication fork pausing and recombination or "gimme a break". *Genes Dev.* 14:1–10.

Schmidt, S.L., X.V. Gomes, and P.M. Burgers. 2001. ATP utilization by yeast replication factor C. III. The ATP-binding domains of Rfc2, Rfc3, and Rfc4 are essential for DNA recognition and clamp loading. *J. Biol. Chem.* 276:34784–34791. http://dx.doi.org/10.1074/jbc.M011633200

Shibahara, K., and B. Stillman. 1999. Replication-dependent marking of DNA by PCNA facilitates CAF-1-coupled inheritance of chromatin. *Cell*. 96:575–585. http://dx.doi.org/10.1016/S0092-8674(00)80661-3

Sikdar, N., S. Banerjee, K.Y. Lee, S. Wincovitch, E. Pak, K. Nakanishi, M. Jasin, A. Dutra, and K. Myung. 2009. DNA damage responses by human

ELG1 in S phase are important to maintain genomic integrity. *Cell Cycle*. 8:3199–3207. http://dx.doi.org/10.4161/cc.8.19.9752

Smith, S., J.Y. Hwang, S. Banerjee, A. Majeed, A. Gupta, and K. Myung. 2004. Mutator genes for suppression of gross chromosomal rearrangements identified by a genome-wide screening in *Saccharomyces cerevisiae*. *Proc. Natl. Acad. Sci. USA*. 101:9039–9044. http://dx.doi.org/10.1073/pnas.0403093101

Smolikov, S., Y. Mazor, and A. Krauskopf. 2004. ELG1, a regulator of genome stability, has a role in telomere length regulation and in silencing. *Proc. Natl. Acad. Sci. USA*. 101:1656–1661. http://dx.doi.org/10.1073/pnas.0307796100

Sporbert, A., A. Gahl, R. Ankerhold, H. Leonhardt, and M.C. Cardoso. 2002. DNA polymerase clamp shows little turnover at established replication sites but sequential de novo assembly at adjacent origin clusters. *Mol. Cell*. 10:1355–1365. http://dx.doi.org/10.1016/S1097-2765(02)00729-3

Sporbert, A., P. Domaing, H. Leonhardt, and M.C. Cardoso. 2005. PCNA acts as a stationary loading platform for transiently interacting Okazaki fragment maturation proteins. *Nucleic Acids Res.* 33:3521–3528. http://dx.doi.org/10.1093/nar/gki665

Su'etsugu, M., and J. Errington. 2011. The replicase sliding clamp dynamically accumulates behind progressing replication forks in Bacillus subtilis cells. *Mol. Cell*. 41:720–732. http://dx.doi.org/10.1016/j.molcel.2011.02.024

Ten Hagen, K.G., D.M. Gilbert, H.F. Willard, and S.N. Cohen. 1990. Replication timing of DNA sequences associated with human centromeres and telomeres. *Mol. Cell. Biol.* 10:6348–6355.

Yang, K., G.L. Moldovan, P. Vinciguerra, J. Murai, S. Takeda, and A.D. D'Andrea. 2011. Regulation of the Fanconi anemia pathway by a SUMO-like delivery network. *Genes Dev.* 25:1847–1858. http://dx.doi.org/10.1101/gad.17020911

Yao, N., J. Turner, Z. Kelman, P.T. Stukenberg, F. Dean, D. Shechter, Z.Q. Pan, J. Hurwitz, and M. O'Donnell. 1996. Clamp loading, unloading and intrinsic stability of the PCNA, beta and gp45 sliding clamps of human, *E. coli* and T4 replicases. *Genes Cells*. 1:101–113. http://dx.doi.org/10.1046/j.1365-2443.1996.07007.x